Gas in Clusters: X-ray and SZE Observations

Max Bonamente, *UAHuntsville and NASA NSSTC*
Esra Bulbul *and* Nicole Hasler, *UAHuntsville*
Marshall Joy, *NASA MSFC*
and collaborators on the Sunyaev-Zeldovich Array project

OUTLINE

- Development of new analytic model of the ICM based on the polytropic equation of state and validation with *Chandra* X-ray and *Sunyaev-Zeldovich Array* observations
- Comparison on X-ray and SZE measurements
- Measurement of the gas fraction independent of cosmology
- Measurement of the Hubble constant
- The effect of He sedimentation on cluster masses

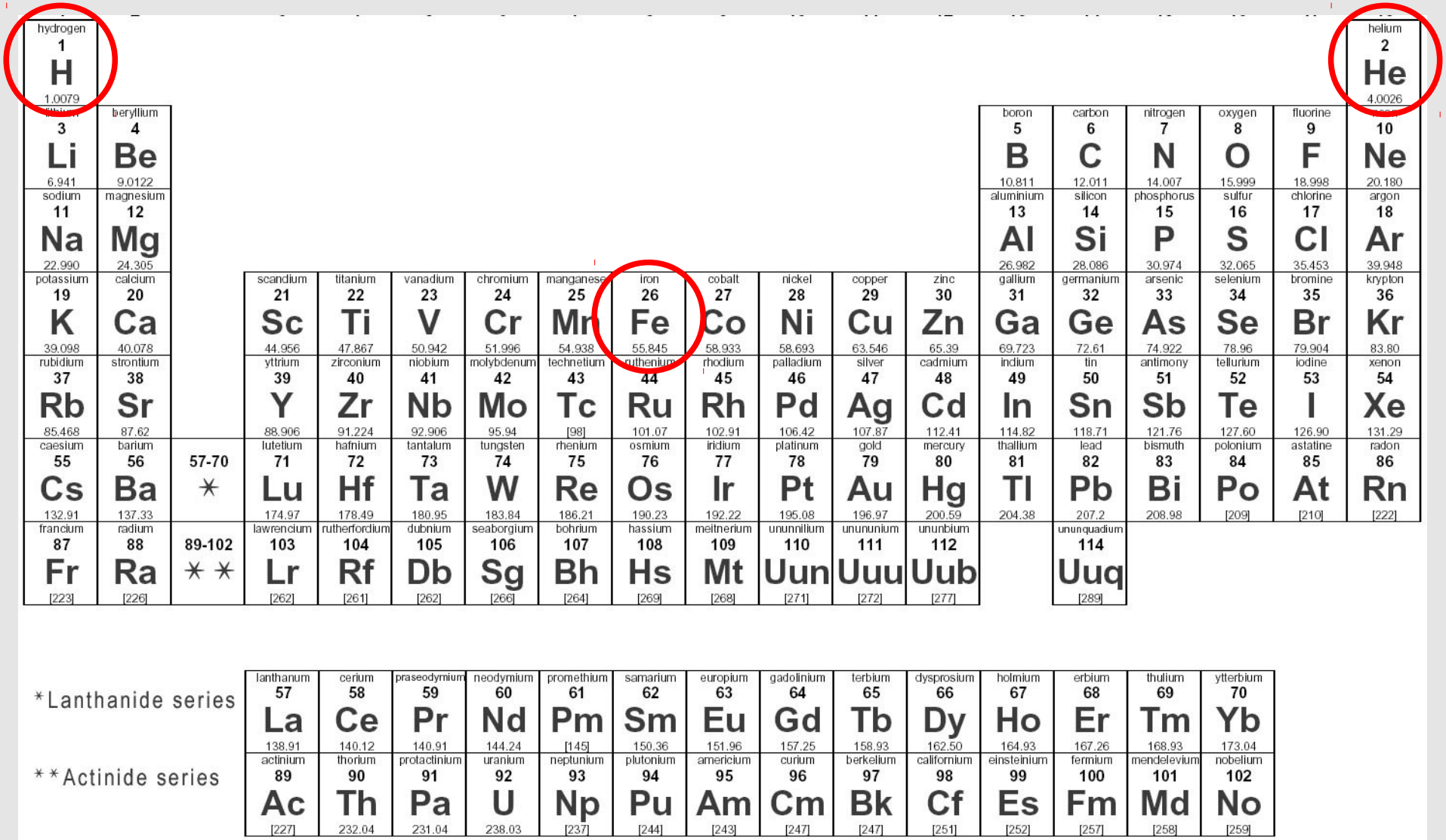
hydrogen 1 H 1.0079
helium 2 He 4.0026
beryllium 4 Be 9.0122
boron 5 B 10.811
carbon 6 C 12.011
nitrogen 7 N 14.007
oxygen 8 O 15.999
fluorine 9 F 18.998
10 Ne 20.180
3 Li 6.941
sodium 11 Na 22.990
magnesium 12 Mg 24.305
aluminium 13 Al 26.982
silicon 14 Si 28.086
phosphorus 15 P 30.974
sulfur 16 S 32.065
chlorine 17 Cl 35.453
argon 18 Ar 39.948
potassium 19 K 39.098
calcium 20 Ca 40.078
scandium 21 Sc 44.956
titanium 22 Ti 47.867
vanadium 23 V 50.942
chromium 24 Cr 51.996
manganese 25 Mn 54.938
iron 26 Fe 55.845
cobalt 27 Co 58.933
nickel 28 Ni 58.693
copper 29 Cu 63.546
zinc 30 Zn 65.39
gallium 31 Ga 69.723
germanium 32 Ge 72.61
arsenic 33 As 74.922
selenium 34 Se 78.96
bromine 35 Br 79.904
krypton 36 Kr 83.80
rubidium 37 Rb 85.468
strontium 38 Sr 87.62
yttrium 39 Y 88.906
zirconium 40 Zr 91.224
niobium 41 Nb 92.906
molybdenum 42 Mo 95.94
technetium 43 Tc [98]
ruthenium 44 Ru 101.07
rhodium 45 Rh 102.91
palladium 46 Pd 106.42
silver 47 Ag 107.87
cadmium 48 Cd 112.41
indium 49 In 114.82
tin 50 Sn 118.71
antimony 51 Sb 121.76
tellurium 52 Te 127.60
iodine 53 I 126.90
xenon 54 Xe 131.29
caesium 55 Cs 132.91
barium 56 Ba 137.33
57-70 *
lutetium 71 Lu 174.97
hafnium 72 Hf 178.49
tantalum 73 Ta 180.95
tungsten 74 W 183.84
rhenium 75 Re 186.21
osmium 76 Os 190.23
iridium 77 Ir 192.22
platinum 78 Pt 195.08
gold 79 Au 196.97
mercury 80 Hg 200.59
thallium 81 Tl 204.38
lead 82 Pb 207.2
bismuth 83 Bi 208.98
polonium 84 Po [209]
astatine 85 At [210]
radon 86 Rn [222]
francium 87 Fr [223]
radium 88 Ra [226]
89-102 **
lawrencium 103 Lr [262]
rutherfordium 104 Rf [261]
dubnium 105 Db [262]
seaborgium 106 Sg [266]
bohrium 107 Bh [264]
hassium 108 Hs [269]
meitnerium 109 Mt [268]
ununnilium 110 Uun [271]
unununium 111 Uuu [272]
ununbium 112 Uub [277]
ununquadium 114 Uuq [289]
*Lanthanide series
lanthanum 57 La 138.91
cerium 58 Ce 140.12
praseodymium 59 Pr 140.91
neodymium 60 Nd 144.24
promethium 61 Pm [145]
samarium 62 Sm 150.36
europium 63 Eu 151.96
gadolinium 64 Gd 157.25
terbium 65 Tb 158.93
dysprosium 66 Dy 162.50
holmium 67 Ho 164.93
erbium 68 Er 167.26
thulium 69 Tm 168.93
ytterbium 70 Yb 173.04
**Actinide series
actinium 89 Ac [227]
thorium 90 Th 232.04
protactinium 91 Pa 231.04
uranium 92 U 238.03
neptunium 93 Np [237]
plutonium 94 Pu [244]
americium 95 Am [243]
curium 96 Cm [247]
berkelium 97 Bk [247]
californium 98 Cf [251]
einsteinium 99 Es [252]
fermium 100 Fm [257]
mendelevium 101 Md [258]
nobelium 102 No [259]

1. Development of a new analytic model of the ICM

Presently, Vikhlinin et al. (2006) and Nagai et al. (2007) models are main options when fitting X-ray and SZE observations

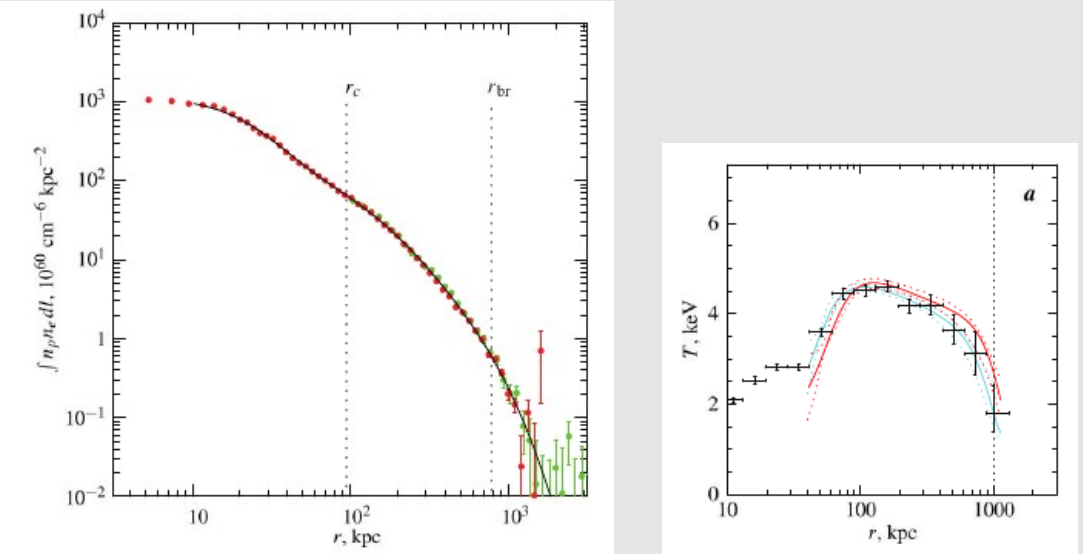

Figure: *The distribution of the surface brightness (left) and temperature (right) for A133 (Vikhlinin et al. 2006)*

Models of density and temperature produce excellent goodness of fit to X-ray data, but are not ideal for a joint modeling of the pressure, which is the Sunyaev-Zeldovich Effect observable.

1.1 The mass density distribution

Assume a mass density (for the total gravitational mass) following a distribution by Suto et al. (1998)

$$\rho_{tot}(r) = \frac{\rho_i}{(r/r_s)(1+r/r_s)^{\beta}}$$

1.2 The gas density and temperature

Use a polytropic equation of state for the hot gas:

$$\frac{n_{e,poly}(r)}{n_{e0}} = \left[\frac{T_{poly}(r)}{T_0}\right]^n$$

1.3 The hydrostatic equilibrium equation

Assume dynamic equilibrium of mass and the hot gas:

$$\frac{1}{\mu m_p n_e(r)}\frac{dP_e}{dr} = -\frac{GM(r)}{r^2}$$

1.4 Modification of equations to account for cooling of gas

The model derived so far is modified by a phenomenological `*core taper*' function (identical to that of Vikhlinin et al. 2006):

$$\tau_{cool}(r) = \frac{\alpha + (r/r_{cool})^{\gamma}}{1 + (r/r_{cool})^{\gamma}}$$

and therefore the temperature and density profiles becomes:

$$\begin{aligned} T(r) &= T_{poly}(r)\tau_{cool}(r) \\ &= T_0 \left(\frac{1}{(\beta-2)} \frac{(1+r/r_s)^{\beta-2} - 1}{r/r_s(1+r/r_s)^{\beta-2}} \right) \frac{\alpha + (r/r_{cool})^{\gamma}}{1 + (r/r_{cool})^{\gamma}} \end{aligned}$$

$$\begin{aligned} n_e(r) &= n_{e,poly}(r)\tau_{cool}^{-1} \\ &= n_{e0} \left(\frac{1}{(\beta-2)} \frac{(1+r/r_s)^{\beta-2} - 1}{r/r_s(1+r/r_s)^{\beta-2}} \right)^{n} \frac{1 + (r/r_{cool})^{\gamma}}{\alpha + (r/r_{cool})^{\gamma}} \end{aligned}$$

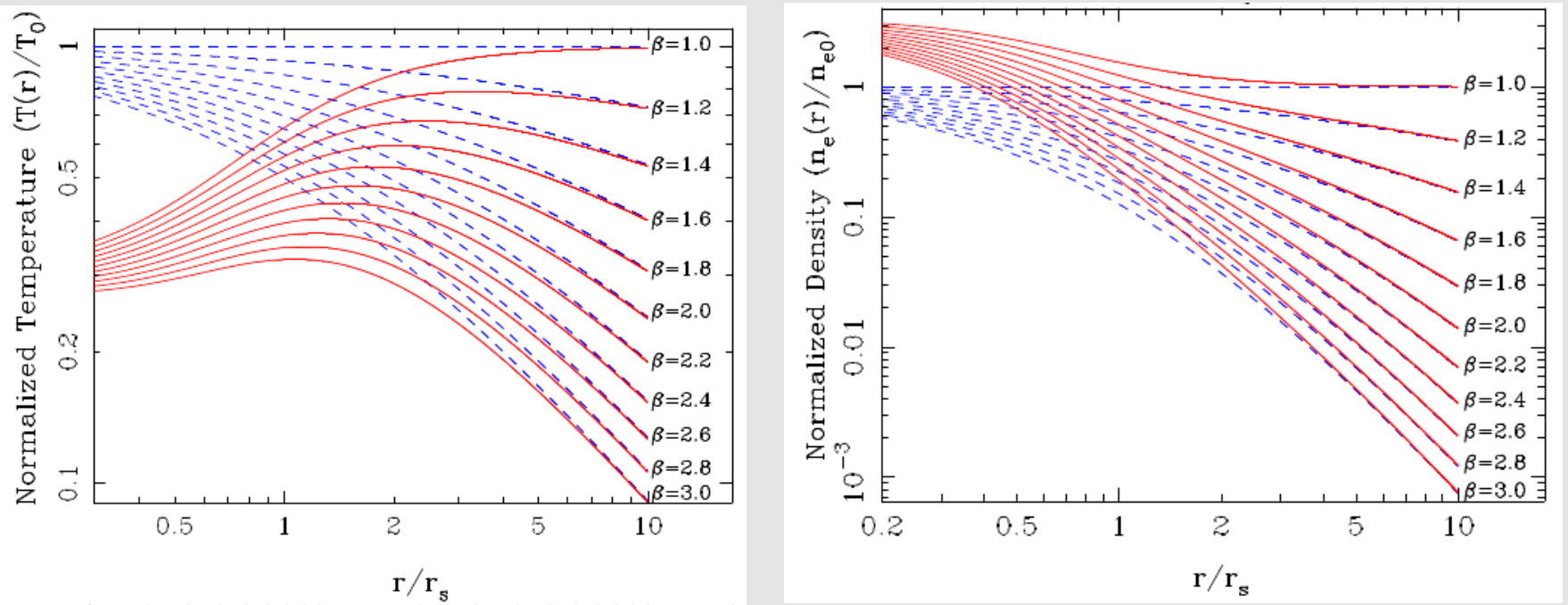

Figure: *The distribution of the temperature and density as function of radius (Bulbul et al. 2010)*

In summary:

3 shape parameters and 2 normalizations for global properties

3 additional parameters for cool-core clusters

2. Validation of the model with Chandra observations

2.1 Application to imaging spectroscopy Chandra observations

Two high S/N observations of Abell 2204 and Abell 1835 are fit well by the model

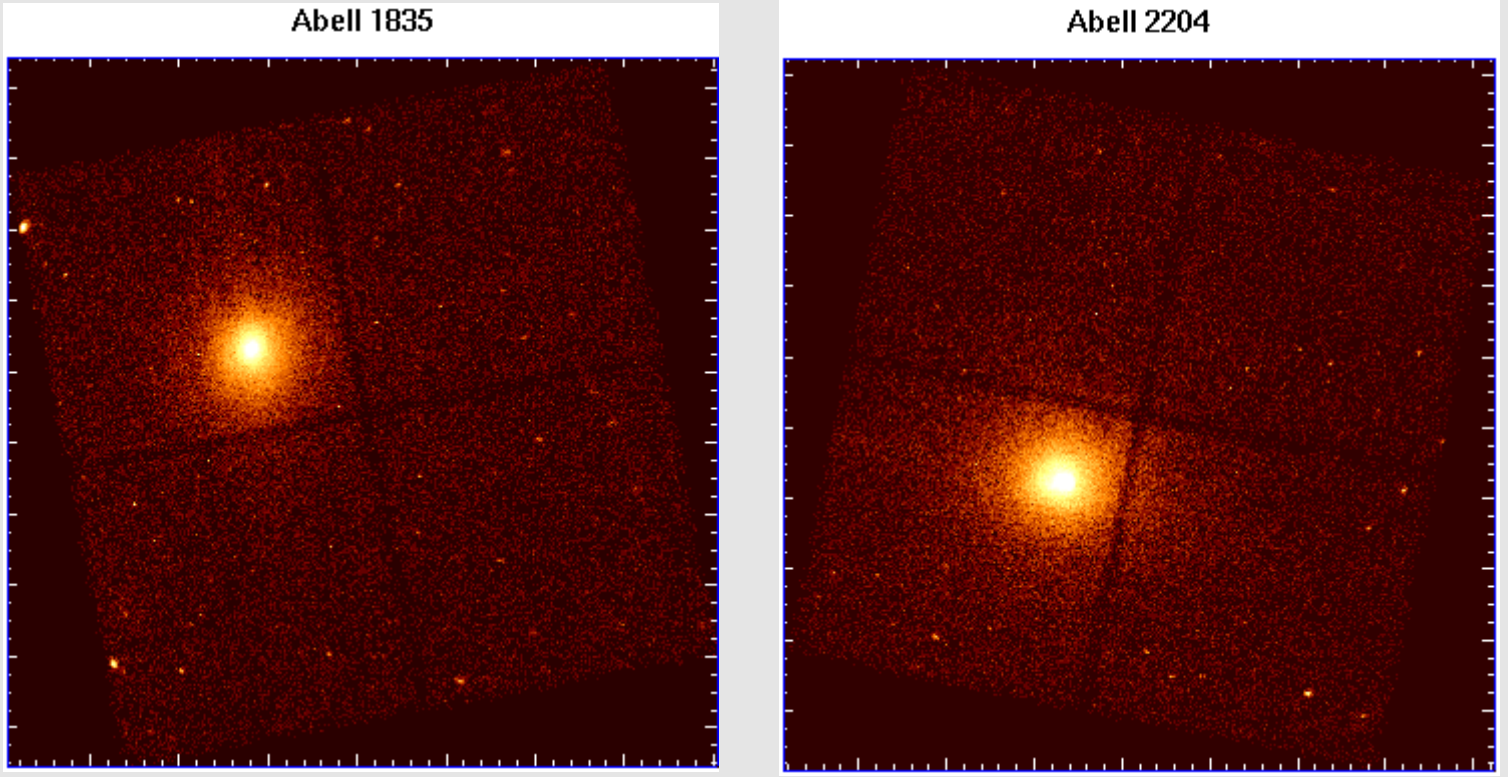

Figure: *Images of Abell 1835 and Abell 2204, 0.7-7 keV band, Chandra observations*

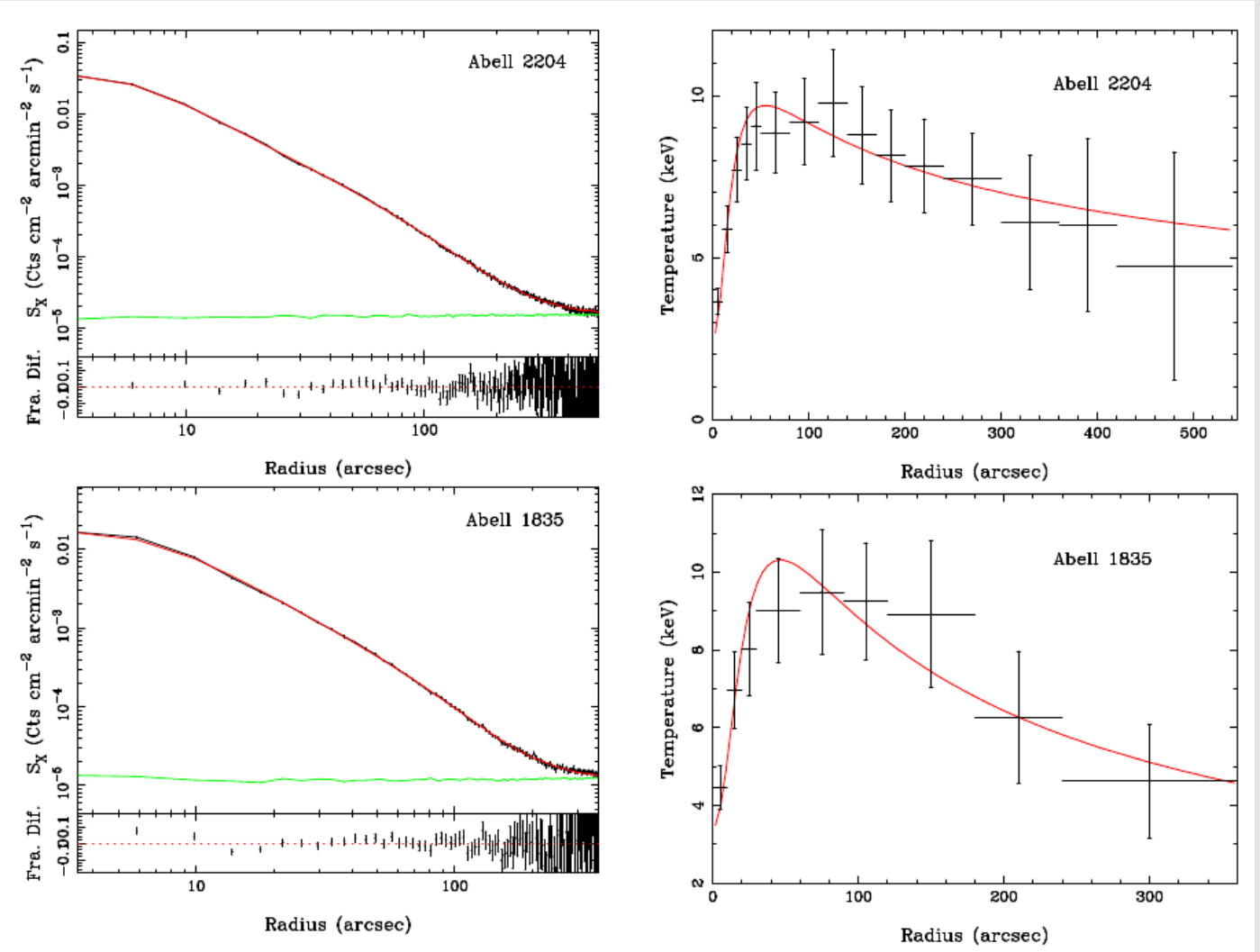

Figure: *Fit of the polytropic model to the surface brightness and temperature profiles (Bulbul et al. 2010)*

3. Application to *Sunyaev-Zeldovich Array* observations

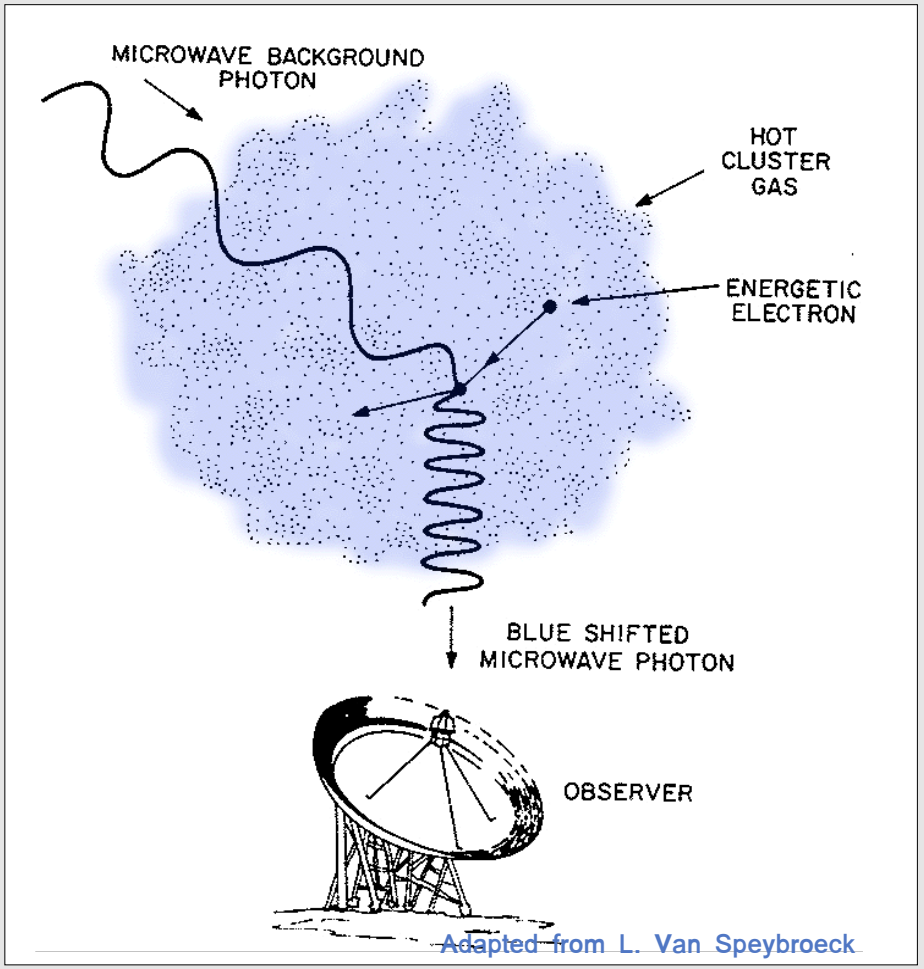

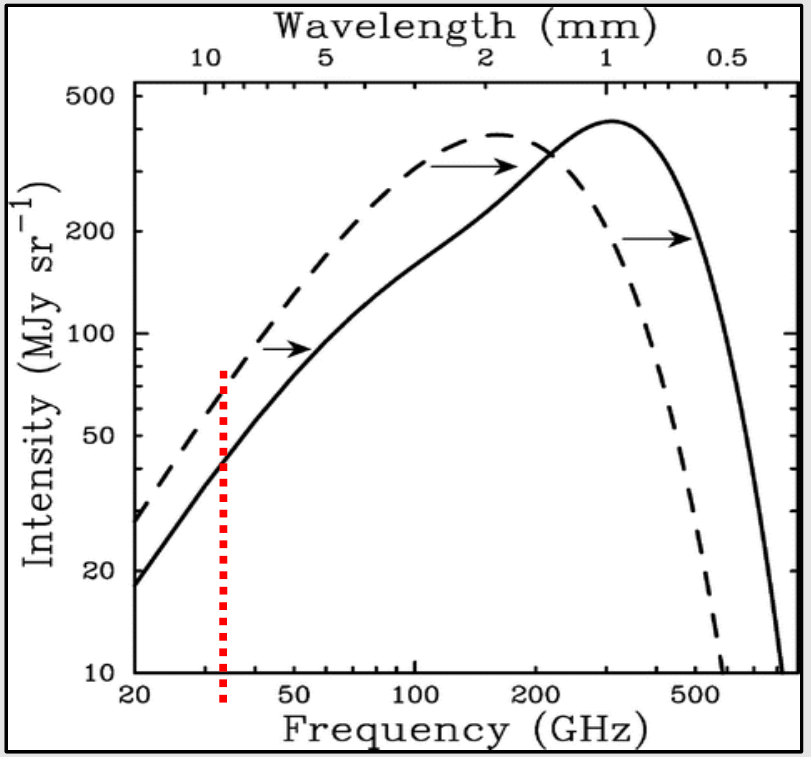

(Credit: Carlstrom et al., (2002)

- Observable: Temperature decrement

$$\Delta T_{CMB} = f_{(x,T_e)} T_{CMB} \int \sigma_T n_e \frac{k_B T_e}{m_e c^2} dl$$

3.1 The *Sunyaev-Zeldovich Array* interferometer

The *SZA* is an 8-element interferometer located in central California, operating at 30 GHz and 90 GHz

Figure: *The SZA interferometric array as part of CARMA, at the Cedar Flats location in California*

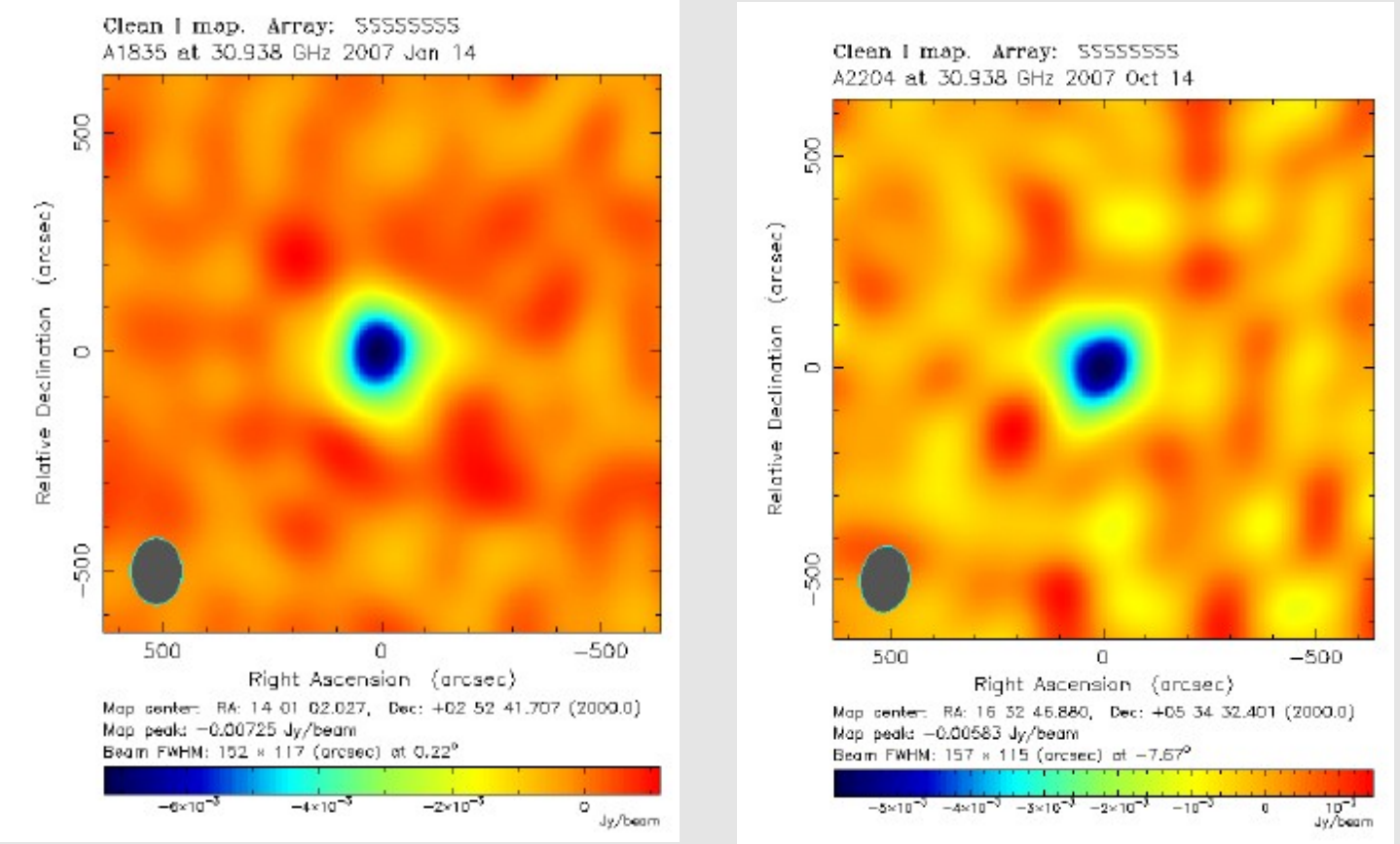

Figure: *SZA images of Abell 1835 and Abell 2204 at 30 GHz (Hasler et al. 2010)*

Joint fit to Chandra and *SZA* data

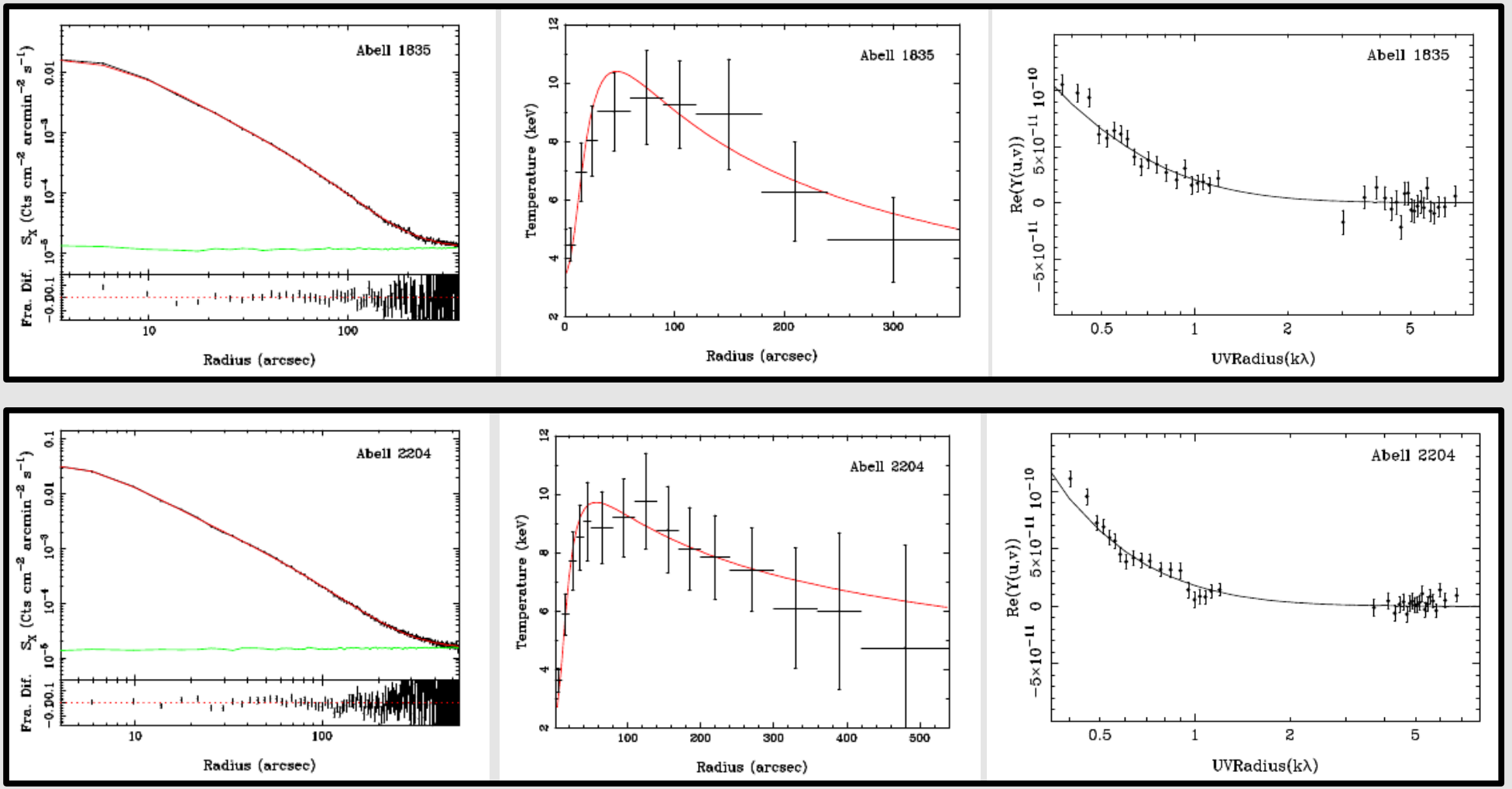

Figure: *Radial plots of surface brightness and temperature (X-ray), and real part of the visibilities as function of (u,v) radius (SZE) for Abell 1835 and Abell 2004 (Hasler et al. 2010)*

3.2 Measurement of masses and distances without priors on cosmology

Joint X-ray and SZE observations results in a unique method of measurement of masses that is cosmology independent:

$$S_{\rm X} = \frac{1}{4\pi(1+z)^4} D_{\rm A} \int n_e(\ell)^2 \Lambda_{ee}(T_e(\ell), A(\ell)) d\ell$$

$$\Delta T_{\rm SZ} = T_{\rm CMB} f(x) D_{\rm A} \int \sigma_{\rm T} n_e(\ell) \frac{k T_e(\ell)}{m_e c^2} d\ell$$

Both density and distance can be measured simultaneously, masses calculated without assuming cosmological parameters .

Cluster	MEASUREMENTS AT R_{2500}				MEASUREMENTS AT R_{500}			
	r_{2500} (")	$M_{\rm gas}$ ($10^{13} M_\odot$)	$M_{\rm tot}$ ($10^{14} M_\odot$)	$f_{\rm gas}$	r_{500} (")	$M_{\rm gas}$ ($10^{13} M_\odot$)	$M_{\rm tot}$ ($10^{14} M_\odot$)	$f_{\rm gas}$
Abell 1835	$152.2 \pm^{27.5}_{22.1}$	$5.49 \pm^{1.28}_{1.15}$	$4.12 \pm^{0.31}_{0.34}$	$0.132 \pm^{0.022}_{0.020}$	$313.6 \pm^{55.8}_{43.9}$	$13.43 \pm^{3.17}_{2.83}$	$7.44 \pm^{0.68}_{0.73}$	$0.180 \pm^{0.037}_{0.031}$
Abell 2204	$182.9 \pm^{32.3}_{25.4}$	$5.24 \pm^{0.87}_{0.74}$	$3.52 \pm^{0.20}_{0.18}$	$0.149 \pm^{0.017}_{0.015}$	$402.4 \pm^{67.6}_{53.1}$	$14.86 \pm^{2.50}_{2.10}$	$7.49 \pm^{0.52}_{0.50}$	$0.200 \pm^{0.022}_{0.022}$

(Hasler et al. 2010)

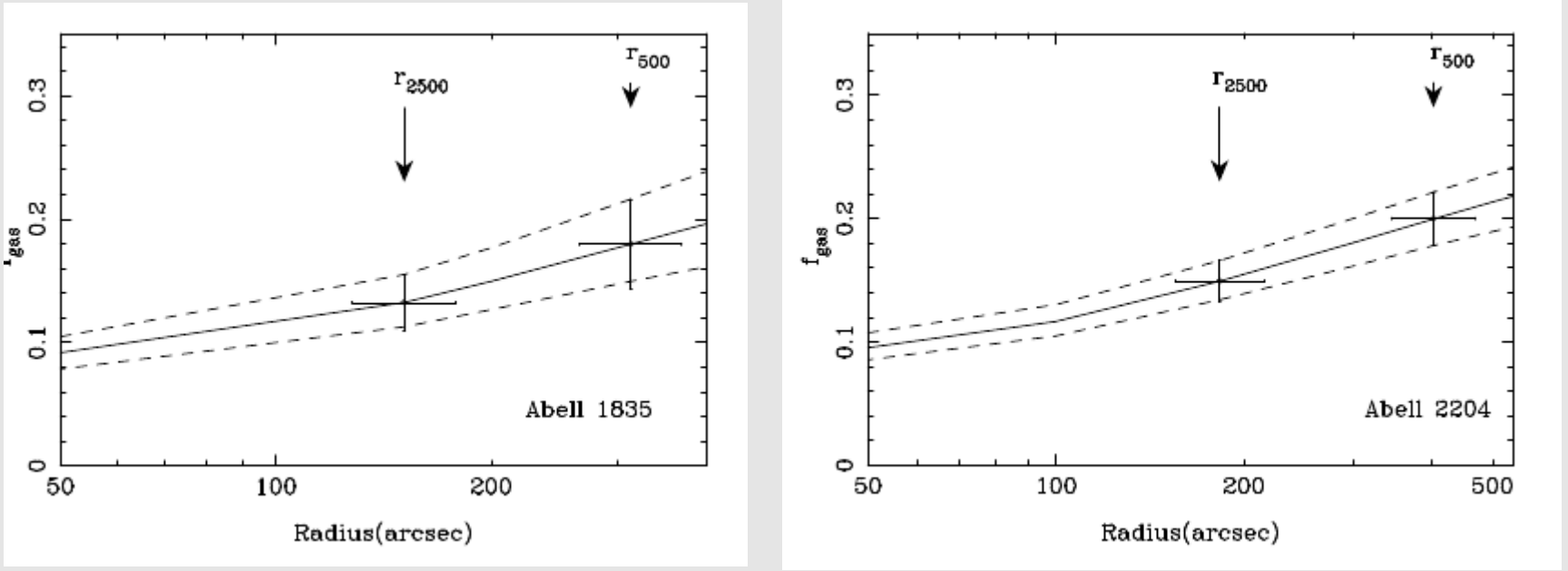

Figure: *Measurement of the gas fraction from joint X-ray and SZE data, for Abell 1835 and Abell 2204 (Hasler et al. 2010)*

If one wants to measure masses at a given density contrast, such as r_{500} , then the calculation of the outer radius carries an uncertainty.

$$M_{\rm tot}(r_\Delta) = 4/3\pi r_\Delta^3 \Delta \rho_c$$

4. Cosmological applications

4.1 Comparison of X-ray and SZE measurements

Comparison between masses inferred from the two observables can be used to determine if X-rays and the SZE observe the same gas (e.g., if there is non-thermal X-ray emission or not)

- In Laroque et al (2006) we measured the gas mass from the two observables (Chandra and OVRO/BIMA data), and found consistent results.
- Good agreement between X-rays and SZ indicated from Chandra and SZA data (Hasler et al. 2010)

- Work by several authors (e.g.,Lieu et al. 2006) from WMAP data reports discrepancy in the analysis of samples of clusters
- Lueker et al (2010) indicate a possible discrepancy between X-ray and SPT power spectrum; more work in progress using Chandra and SPT observations of individual clusters.

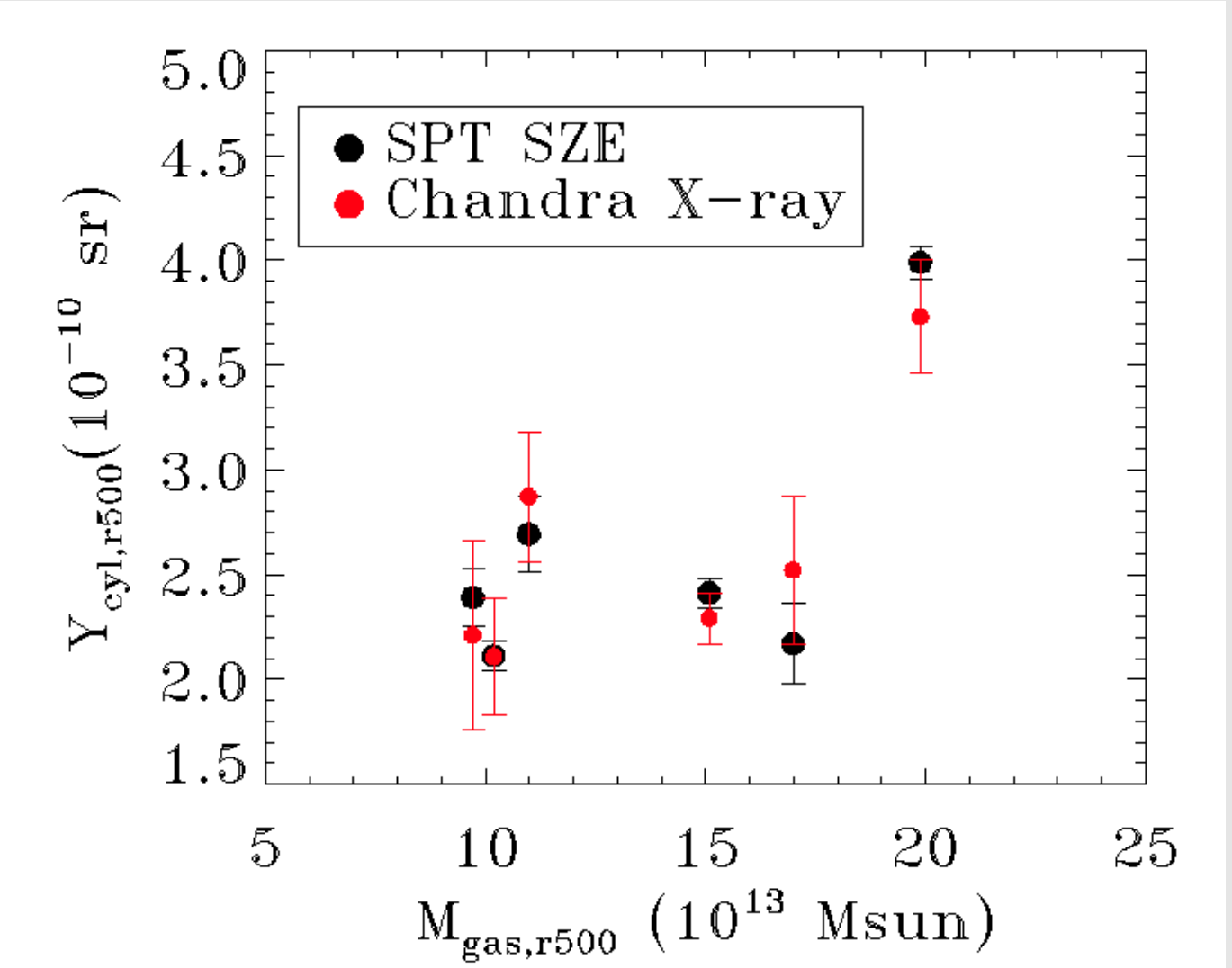

Figure: preliminary results on the Chandra/SPT Comparison (Plagge et al. 2011)

4.2 Use of the gas fraction template for cosmology

Work in progress on the measurement of the gas fraction independent of cosmology, for a sample of 30 clusters at z=0.1-1.1.

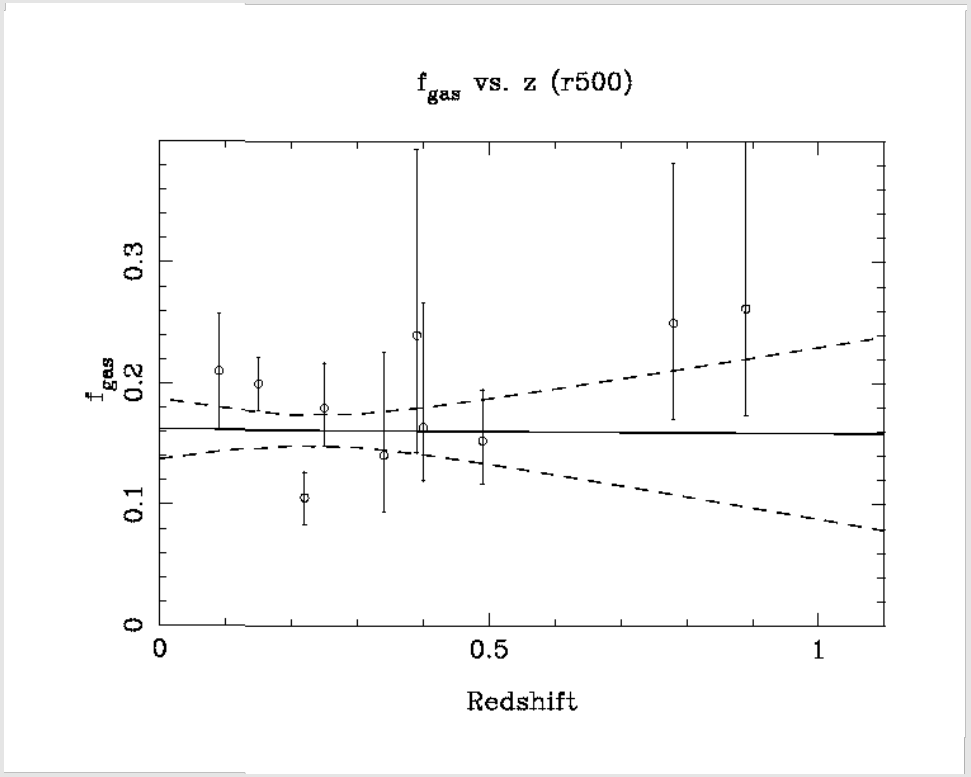

Knowing the distribution of f_{gas} as function of redshift can be used to constrain dark energy (Sasaki 1996, Pen 1997, Allen et al. 2008, Ettori 2009).

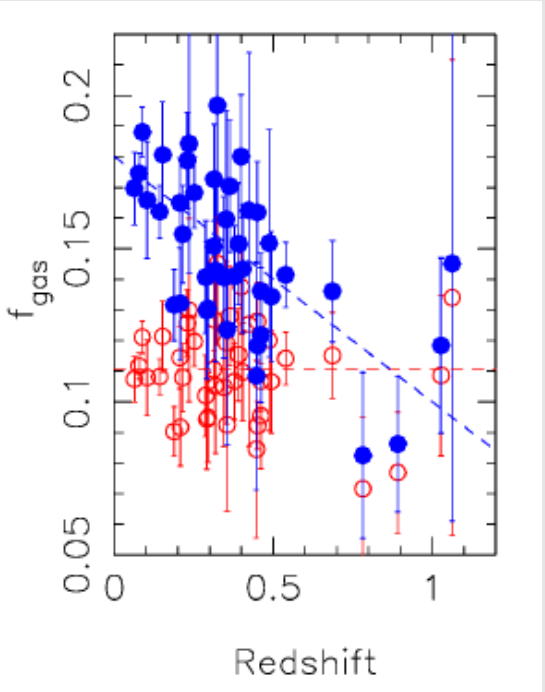

Figure: *The X-ray method of measuring masses depends on cosmology (from Allen et al. 2008)*

4.3 Measurement of the Hubble constant

Using $D_A(z)$ information alone, the measurement of the Hubble constant depends on priors on Ω_Λ.

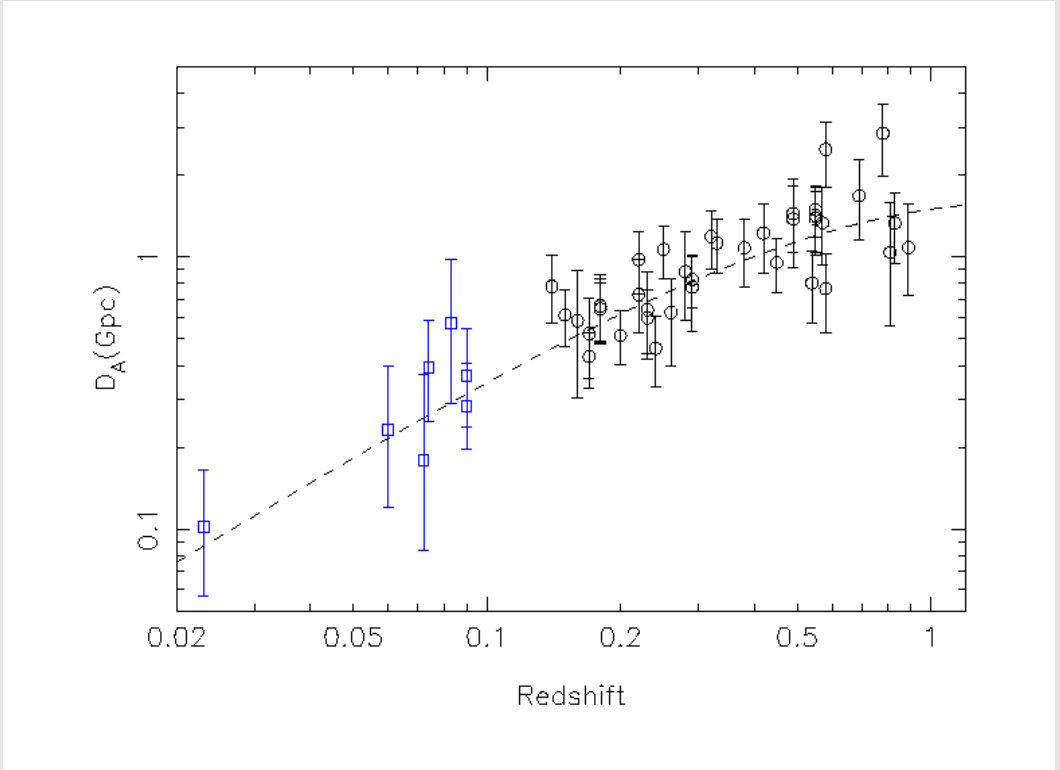

$$H_0 = 76.9 \pm^{3.9}_{3.4} \pm^{10.0}_{8.0} (\chi^2 = 31.6)$$

$$\Omega_M = 0.3,\ \Omega_\Lambda = 0.7$$

$$H_0 = 67.1 \pm^{4.5}_{3.6} \pm^{10.0}_{8.0} (\chi^2 = 32.5)$$

$$\Omega_M = 1.0,\ \Omega_\Lambda = 0.0$$

Figure: *Measurement of the Hubble constant from earlier OVRO/BIMA observations (Bonamente et al. 2006)*

Work in progress on a sample of 30 clusters at z=0.1-1.1...

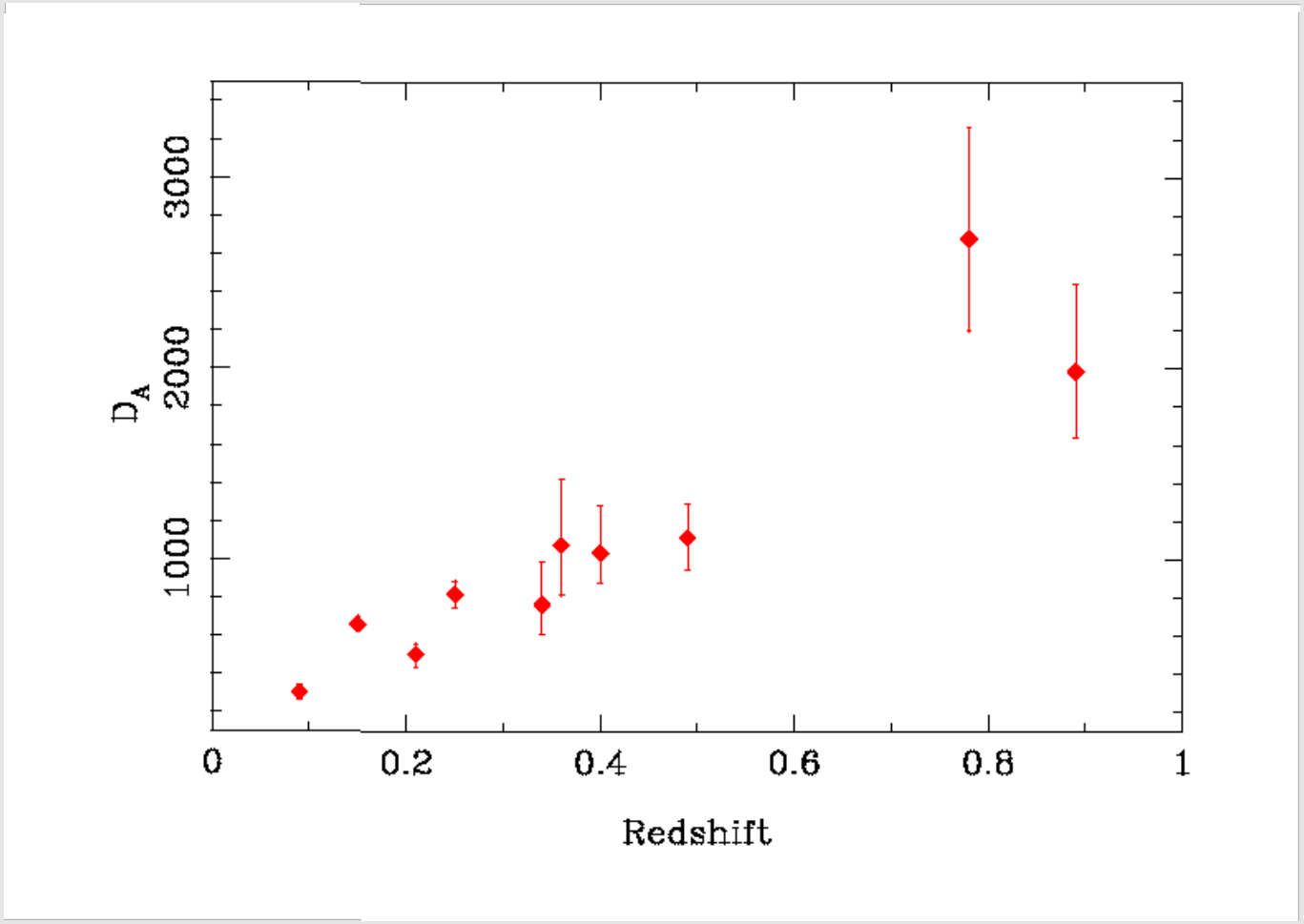

4.4 The effect of He sedimentation on cluster masses

Radial gradients of He (and other elements) can lead to biases in the measurement of cluster masses

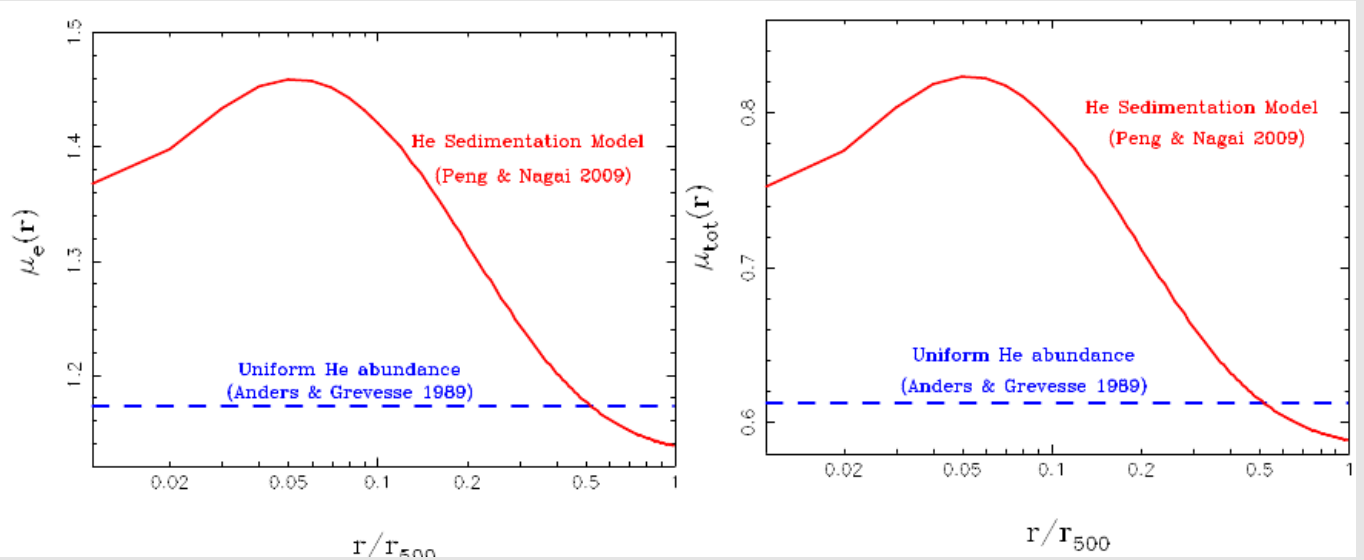

Figure:Effect of the Peng & Nagai 2009 He sedimentation model on mean molecuar numbers *(Bulbul et al. 2010)*

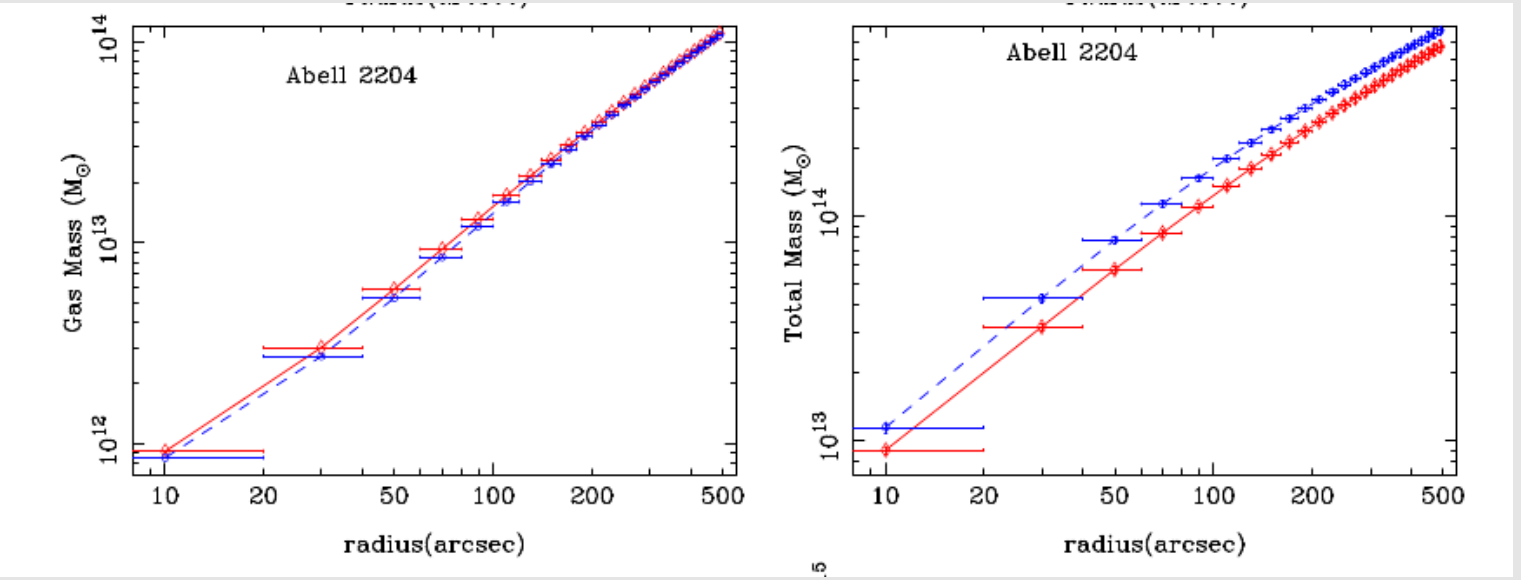

Figure:Effect of the Peng & Nagai 2009 He sedimentation model on cluster masses *(Bulbul et al. 2010)*

Actual *measurement* of He sedimentation can be obtained by combining X-ray and SZE observations, though very challenging at present.

CONCLUSIONS

- We developed and validated a new model for the analysis of X-ray and SZE observations of galaxy clusters.
- The model is especially designed for applications in which both X-ray and SZE observations must be modeled simultaneously
- Applications include the measurement of gas fraction independent of cosmology, constraints on Hubble constant and dark energy, and the sedimentation of heavy ions

3.3 Comparison of new model with Nagai et al. (2007) model

Two models provide equally acceptable fits, and measure the same Y, by using the same number of degrees of freedom.

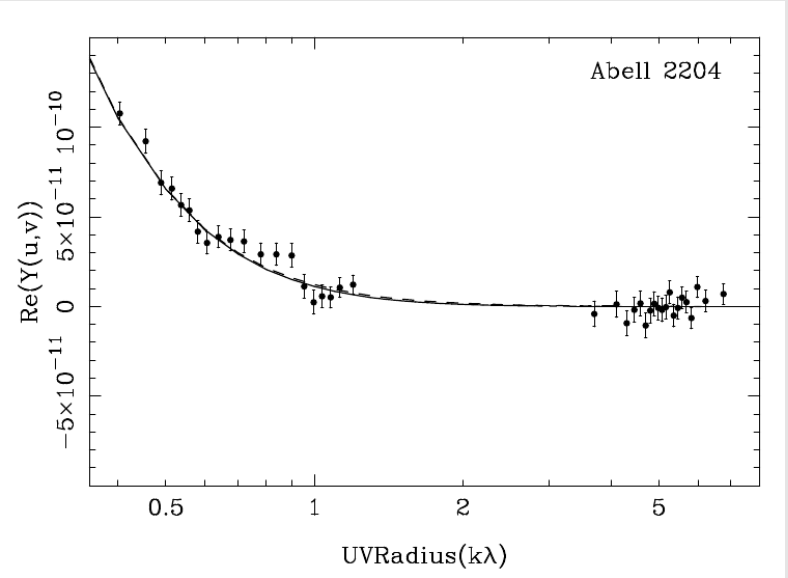

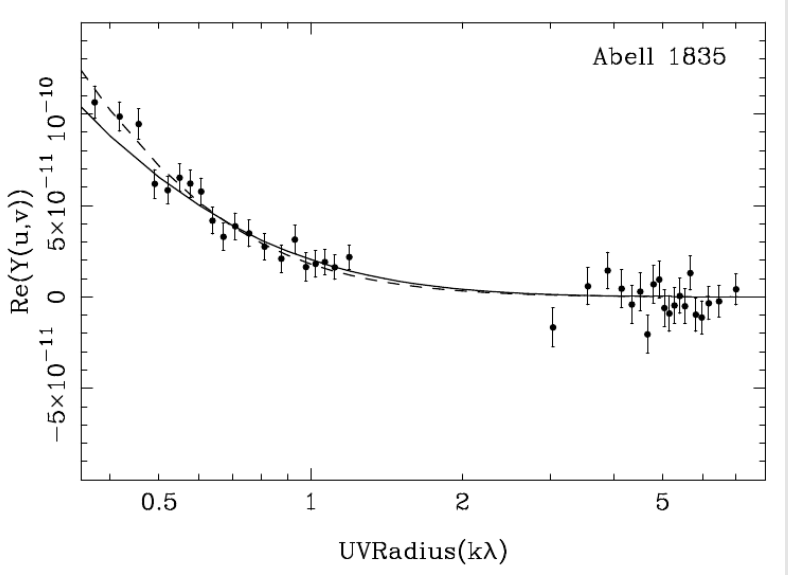

Cluster	$Y_{cyl}(10^{-5})$
Abell 1835	
Poly	$9.90\pm^{0.85}_{0.78}$
N08	$10.01\pm^{0.84}_{0.76}$
Abell 2204	
Poly	$5.57\pm^{0.60}_{0.52}$
N08	$6.05\pm^{0.80}_{0.64}$

3.4 Preliminary comparison of with Vikhlinin et al. (2006) model

Bulbul et al. (2010)

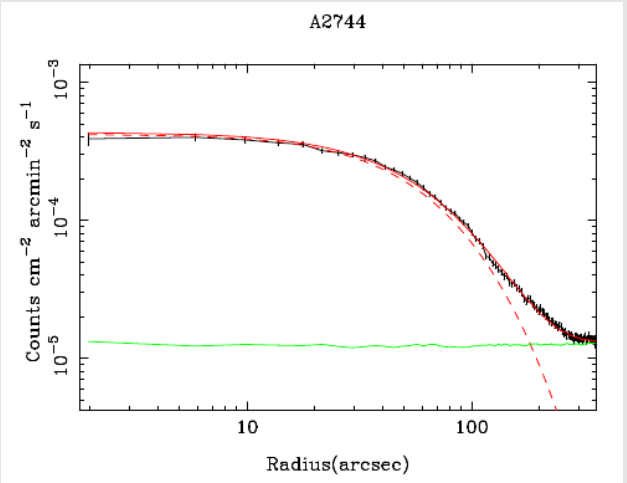

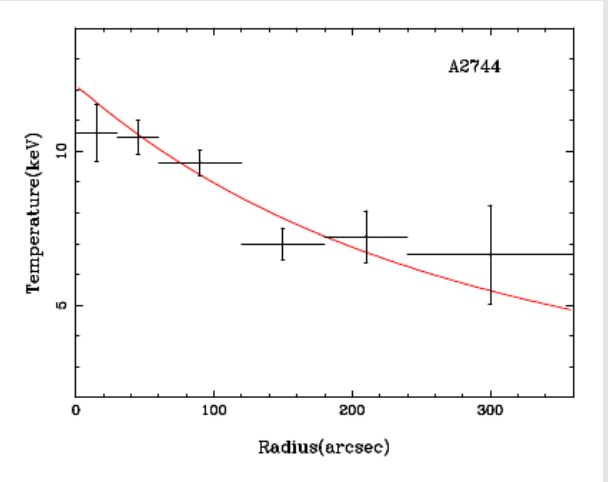

(5 model parameters)

Vikhlinin et al. (2006)

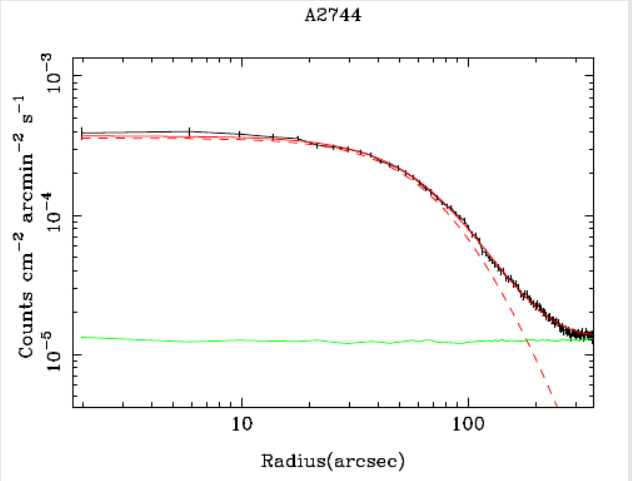

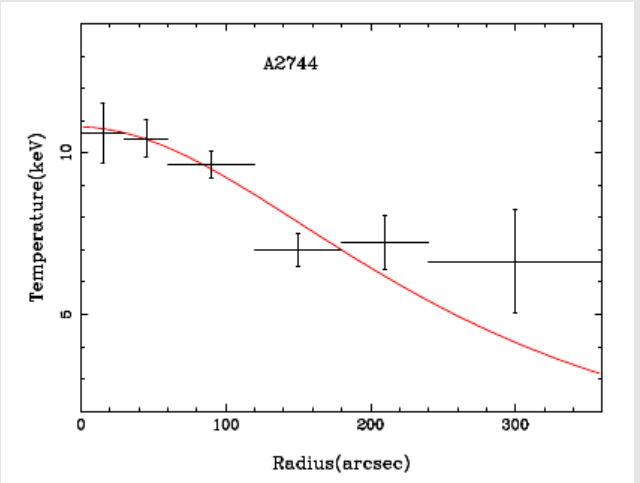

(7 model parameters)